The Journal of Prevention of Alzheimer's Disease 12 (2025) 100030

Contents lists available at ScienceDirect

The Journal of Prevention of Alzheimer's Disease

journal homepage: www.elsevier.com/locate/tjpad

Original Article

Basal forebrain global functional connectivity is preserved in asymptomatic presenilin-1 *E280A* mutation carriers: Results from the Colombia cohort

Alice Grazia[a,*], Martin Dyrba[b], Nunzio Pomara[c], Anna G. Temp[d], Michel J. Grothe[e], Stefan J. Teipel[a,b], for the Alzheimer's Prevention Initiative (API) Autosomal-Dominant Alzheimer's Disease (ADAD) Trial

[a] *Department of Psychosomatic Medicine, University Medicine Rostock, Rostock, Germany*
[b] *Deutsches Zentrum für Neurodegenerative Erkrankungen (DZNE), Greifswald, Rostock, Germany*
[c] *Geriatric Psychiatry Division of Nathan S, Kline Institute, New York, USA*
[d] *Neurozentrum, BG Klinikum Hamburg GmbH, Germany*
[e] *Reina Sofia Alzheimer's Center, CIEN Foundation, ISCIII, Spain*

ARTICLE INFO

Keywords:
Basal forebrain
PSEN1 E280A
Colombia cohort
Resting-state fMRI
Bayesian analysis

ABSTRACT

Background: Imaging studies showed early atrophy of the cholinergic basal forebrain in prodromal sporadic Alzheimer's disease and reduced posterior basal forebrain functional connectivity in amyloid positive individuals with subjective cognitive decline. Similar investigations in familial cases of Alzheimer's disease are still lacking.
Objectives: To test whether presenilin-1 E280A mutation carriers have reduced basal forebrain functional connectivity and whether this is linked to amyloid pathology.
Design: This is a cross-sectional study that analyzes baseline functional imaging data.
Setting: We obtained data from the Colombia cohort Alzheimer's Prevention Initiative Autosomal-Dominant Alzheimer's Disease Trial.
Participants: We analyzed data from 215 asymptomatic subjects carrying the presenilin-1 E280A mutation [64% female; 147 carriers (M = 35 years), 68 noncarriers (M = 40 years)].
Measurements: We extracted functional magnetic resonance imaging data using seed-based connectivity analysis to examine the anterior and posterior subdivisions of the basal forebrain. Subsequently, we performed a Bayesian Analysis of Covariance to assess the impact of carrier status on functional connectivity in relation to amyloid positivity. For comparison, we also investigated hippocampus connectivity.
Results: We found no effect of carrier status on anterior (Bayesian Factor$_{10}$ = 1.167) and posterior basal forebrain connectivity (Bayesian Factor$_{10}$ = 0.033). In carriers, we found no association of amyloid positivity with basal forebrain connectivity.
Conclusions: We falsified the hypothesis of basal forebrain connectivity reduction in preclinical mutation carriers with amyloid pathology. If replicated, these findings may not only confirm a discrepancy between familial and sporadic Alzheimer's disease, but also suggest new potential targets for future treatments.

1. Introduction

The basal forebrain is the central site of cholinergic projections to the cerebral cortex and limbic system, and it is considered a key player in the neuropathology of early Alzheimer's Disease (AD) [1,2]. Imaging studies have shown that this brain region is severely atrophied in sporadic AD dementia and may even precede medial temporal lobe degeneration in the prodromal phase of AD [3,4]. Recently, resting-state functional connectivity studies facilitated the functional distinction of basal forebrain subdivisions [5,6]. Specifically, an anterior-medial subdivision characterized by connectivity with the hippocampus and nodes of the medial cortical memory network, and a posterior-lateral subdivision connected with nodes of the Salience Network (e.g., anterior insula, dorsal anterior cingulate) [5]. Subsequently, one study showed that connectivity alterations of the posterior basal forebrain subdivision occurred in individuals with subjective cognitive complaints and in association with amyloid pathology [7]. The same study found that resting-state functional connectivity in the posterior basal forebrain was significantly negatively correlated with amyloid uptake, while no significant correlations were found for the anterior basal forebrain subdivision [7]. This suggests that

* Corresponding author at: Department of Psychosomatic Medicine, University of Rostock, Gehlsheimer Str. 20, 18147 Rostock, Germany.
E-mail address: alice.grazia@med.uni-rostock.de (A. Grazia).

https://doi.org/10.1016/j.tjpad.2024.100030
Received 26 September 2024; Received in revised form 5 November 2024; Accepted 2 December 2024
Available online 1 January 2025

amyloid-related connectivity reductions may be more pronounced in the posterior subdivision of the basal forebrain, leading us to hypothesize a similar pattern in presenilin-1 (*PSEN1*) E280A carriers [7]. However, similar analyses in familial cases of AD are still lacking.

Autosomal-Dominant Alzheimer's Disease (ADAD) accounts for 1–2 % of all AD cases and has a dramatically early onset [8]. Therefore, studying this population represents a unique opportunity to gain more insights into early-onset familial AD. This disease is primarily caused by genetically inherited mutations of the *PSEN1*, presenilin2 (*PSEN2*), and amyloid precursor protein (APP) [8]. Although ADAD and AD arise from different genetic and biological processes, they share neuropathological and clinical features [8]. The first case of early-onset ADAD with a single *PSEN1* mutation at codon 280 (E280A), which likely originated from a single founder, was described in 1987 in Colombia [9]. Since then, many other Colombian families with the same mutation have been identified and screened. Alzheimer's Disease due to *PSEN1 E280A* mutation typically presents with gradual memory loss, followed by changes in behavior and language impairment [10]. The patterns of amyloid β deposition in *PSEN1* E280A cases are very similar to those of sporadic AD [11]. In *PSEN1 E280A* mutations, amyloid deposition supposedly starts at age 28 [12], while clinical manifestations occur at a median age of 44 years for mild cognitive impairment (MCI) and at a median age of 49 years for dementia [10,12,13]. Carriers of *PSEN1 E280A* typically die at a median age of 59 years [10]. Studies investigating resting-state networks in ADAD yielded complex and divergent results [14], with some reporting reduced functional connectivity in nodes of the Default Mode Network (DMN) [15,16], and others reporting patterns of increased functional connectivity in the DMN and frontostriatal circuits [17].

Our study aim was twofold. Firstly, we wanted to investigate cholinergic basal forebrain functional connectivity in asymptomatic *PSEN1* mutation carriers compared to noncarriers. Secondly, we wanted to study the association of basal forebrain connectivity with amyloid pathology in asymptomatic *PSEN1* mutation carriers based on amyloid PET data. To complement our analysis, we included the hippocampus as a comparison region, given its well-established involvement in early Alzheimer's disease pathology and its known vulnerability to amyloid deposition and connectivity changes [3,18,19]. By including the hippocampus, we aimed to assess whether changes in basal forebrain connectivity would parallel or differ from those observed in this key region of memory processing. Our primary hypothesis was that basal forebrain and hippocampal functional connectivity would be significantly reduced in carriers compared to noncarriers, with posterior-lateral basal forebrain connectivity being more reduced than anterior-medial basal forebrain connectivity. This was based on findings from the abovementioned preclinical sporadic AD study showing that amyloid-related reductions were more pronounced in the posterior subdivision [7]. As a secondary hypothesis, we expected to find reduced basal forebrain and hippocampal functional connectivity in mutation carriers with increased levels of amyloid.

2. Methods

We requested the publicly available baseline data from the Alzheimer's Prevention Initiative (API) Autosomal-Dominant Alzheimer's Disease Colombia Trial (NCT01998841, date of registration: November 22, 2013) [20] approved by the Colombian Health Authority (Instituto Nacional de Vigilancia de Medicamento). This is a prospective, randomized, double-blind, placebo-controlled study of the efficacy of crenezumab versus placebo in asymptomatic *PSEN1 E280A* mutation carriers from the same family kindred with ADAD in Colombia. The rationale and design of this study are described in detail elsewhere [11,20]. Informed consent was acquired from all study participants and study partners. All consent procedures were conducted in compliance with the requirements of international and local ethics committees and after the ethics committees' approval [11].

2.1. Participants

The study recruited individuals carrying the *PSEN1 E280A* autosomal-dominant mutation [21] between the age of 30–60 years. Of the initial 252 enrolled participants, 10 participants' data had to be excluded from the baseline dataset for confidentiality reasons [22]. Noncarriers' controls included individuals of the same kindred matched for age and sex. All participants needed to be cognitively unimpaired or asymptomatic to be included in the study. Details about inclusion and exclusion criteria are published in the study protocol [11].

2.2. Brain imaging acquisition

Participants were scanned using a Siemens 1.5T Avanto scanner at the Hospital Pablo Tobón Uribe (Medellín, Colombia) after cognitive screening but before PET amyloid imaging. All participants were instructed to keep their eyes open and stay awake for the whole duration of the scan (10:08 min). High-resolution anatomical images were acquired using a 3D T1-weighted Magnetization-Prepared Rapid Acquisition Gradient Echo (MP-RAGE) sequence in the sagittal plane according to the following sequence parameters: repetition time = 1800 ms; echo time = 2.5 ms; inversion time = 900 ms; flip angle = 10°; 172 sagittal slices with matrix size = 192 × 192; field of view (FOV) = 240 mm; slice thickness = 1.2 mm; in-plane spatial resolution (voxel size): 1.25 mm × 1.25 mm. The structural images were used for co-registration with the functional MRI (fMRI) data for the subsequent analyses. Resting-state fMRI sequences were angulated parallel to anterior and posterior commissure (AC-PC) line, then tilted 15° toward the top of the head, and acquired according to the following parameters: 39 axial slices with a matrix size = 70 × 70, in-plane spatial resolution (voxel size) = 3 mm × 3 mm, slices thickness = 4 mm, repetition time (TR) = 3000 ms, echo time (TE) = 30 ms, flip angle = 80°, field of view (FOV) = 210 mm. PET scans were acquired on a Siemens Biograph PET/CT, using an intravenous (IV) bolus injection of ~11 mCi (9.3–14.7 mCi) of florbetapir (AV45), a CT scan for correction of radiation attenuation, a 50-minute radiotracer uptake-period, and a 20-minute dynamic emission scan in four frames (4 × 300 s). Then, PET images were reconstructed using an OSEM algorithm and attenuation-corrected, frames were evaluated for adequate count statistics and absence of head motion [12].

2.3. Imaging data pre-processing

We pre-processed resting-state fMRI data with the toolbox Data Processing Assistant for resting-state fMRI (DPARSF; Advanced Edition, version 5.2) implemented in MATLAB R2020a (MathWorks, Natick, MA) in conjunction with the statistical parametric mapping software (SPM12, Welcome Trust Center for Neuroimaging, https://www.fil.ion.ucl.ac.uk/spm/). We excluded the first 10 time points to allow magnetic signal stabilization and participants' adaptation to the scanning noise. We performed slice-timing correction and realignment to remove timing differences and head movement artifacts. We first co-registered anatomical T1-weighted images with the mean of the functional images. The T1-weighted images were subsequently segmented into gray matter (GM), white matter (WM), and cerebrospinal fluid (CSF) and spatially normalized to Montreal Neurological Institute (MNI) space using Diffeomorphic Anatomical Registration Through Exponentiated Lie Algebra (DARTEL; Ashburner, 2007). For the functional data, we replicated the design of two previous studies investigating basal forebrain functional connectivity [5,7]. Consequently, we regressed out mean WM, CSF, global signal (GSR), and 24 head motion parameters [23] as nuisance variables. We opted for GSR as denoising method over other principal components-based methods (e.g., aCompCor) due to its effectiveness in reducing global noise across voxels, which is advantageous in seed-based analyses, particularly for enhancing sensitivity to neural activity in our regions of interest. Moreover, we wanted to stay

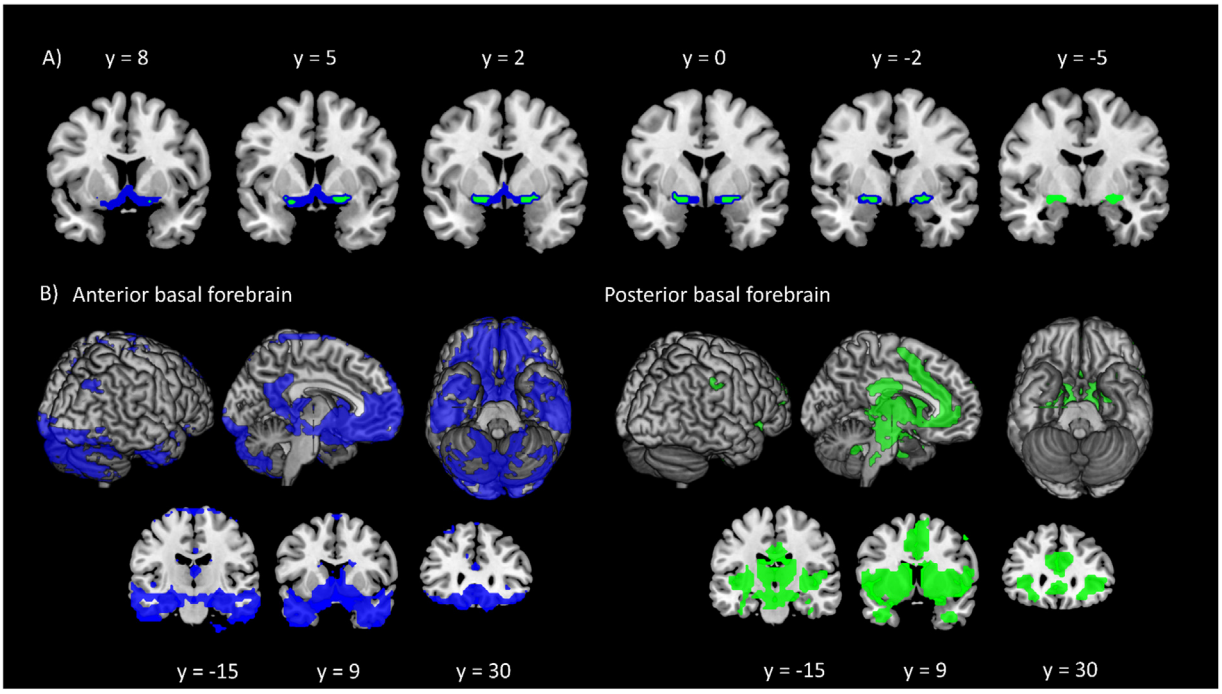

Fig. 1. Basal forebrain parcellation and functional connectivity. **A**) Coronal slices showing anterior-medial (blue) and posterior-lateral (green) clusters of basal forebrain. Slice positions follow the Montreal Neurological Institute (MNI) y-coordinates. **B**) Corresponding functional connectivity networks of anterior basal forebrain and posterior basal forebrain seeds (p (FWE) < 0.05) are depicted on lateral, medial and ventral brain surfaces as well as on representative coronal sections at MNI coordinates: $y = -15$, $y = 9$, $y = 30$.

consistent with our previous pipelines, in which we assessed the basal forebrain functional connectivity profiles within the Alzheimer's disease continuum [5,6], to facilitate comparability between cohorts. Also, we found GSR to be very effective in reducing motion effects, especially in clinical populations. A recent study comparing denoising methods demonstrated that the Independent Component Analysis for Automatic Removal of Motion Artifacts (ICA -AROMA) and GSR were the most effective in removing physiological noise, followed by CompCor [24]. Another study indicated that the use of CompCor resulted in the introduction of high-frequency noise [25]. Nonetheless, considering that GSR can induce negative correlations and spurious effects [26,27], or even remove information relevant to brain functional connectivity [27], we conducted a sensitivity analysis including the global signal (see Supplementary materials).

Subsequently to denoising, we filtered the images using a band-pass filter (0.1–0.01 Hz) to remove the effects of high-frequency noise and signal drift. Then, the fMRI data were projected to MNI space by applying the respective deformation fields of the T1-weighted images and resampled to 3 × 3 × 3 mm voxels. Finally, the functional data was smoothed with a 4 mm Gaussian kernel. We manually checked for residuals of head motion artifacts, and excluded subjects using the mean of frame-wise displacement (FD) [28] and considering values above 0.2 mm as above the norm for healthy adults [29].

2.4. Regions of interest, global functional connectivity and regional homogeneity analysis

We selected anterior-medial and posterior-lateral basal forebrain, as well as left/right hippocampus as seed regions of interest (ROIs) to test our a priori hypothesis. The basal forebrain subdivisions were based on previous studies [5,6] that identified differential patterns of functional connectivity of the cholinergic basal forebrain based on its anterior and posterior subdivisions (Fig. 1 A). A detailed description of the basal forebrain connectivity-based parcellation methodology can be found elsewhere [5]. We defined right and left hippocampus ROIs in MNI space based on the Harvard-Oxford atlas, which was masked to include only the GM. We then resampled these masks to a final voxel size of 3 mm isotropic to match the voxel size of the resting-state-fMRI images. For the anterior-medial and posterior-lateral basal forebrain ROIs as well as the right/left hippocampus ROIs, we generated resting-state functional connectivity (RSFC) maps by correlating the ROIs' mean signal time course with all other GM voxels of the brain (Fig. 1 B). RSFC maps were then Fisher z-transformed. In order to restrict the analysis to specific RSFC networks, we first estimated the basal forebrain and hippocampus network masks over all subjects. This was done using a one-sample *t*-test over all subjects (covariates: age, sex, CDR score, *APOE* ε4 status and years of education) applying a p-value threshold = 0.05 corrected for family-wise error (FWE), an extent threshold of 10 and a minimum cluster-size of 20. The resulting network outlines (Fig. 1 B) were binarized and added as masks for the subsequent second-level analysis. To corroborate the robustness of our analysis, we conducted a sensitivity analysis wherein we constructed the basal forebrain networks from the data of healthy subjects and then applied them to the data of carriers and non-carriers, which demonstrated no discernible differences (Additional File 1).

The second-level analysis included two separate full factorial models performing multiple regressions to assess the effect of mutation status and amyloid burden on the RSFC maps. The first model included *PSEN1 E280A* mutation status as a predictor variable and age, sex, CDR scores, *APOE* ε4 status and years of education as covariates. The second model carried out in the carriers group only, included amyloid status as a predictor variable and age, sex, CDR scores, *APOE* ε4 status and years of education as covariates. Contrasts were defined as follows: contrast 1: carriers > noncarriers; contrast 2: carriers < noncarriers; contrast 3: amyloid positive < amyloid negative. To visualize our results, we used the toolbox bspmview implemented in SPM and applied the following parameters for visualization: p-value = 0.01, uncorrected for multiple comparisons, and extend threshold = 10. Since the RSFC maps resulting from the factorial models did not survive multiple comparisons correction (FWE, FDR), we additionally computed seed-based global

functional connectivity (GFC) [30] of posterior/anterior basal forebrain and left/right hippocampus to test our hypothesis with the Bayesian methodology. GFC, as a measure of functional connectivity strength, is a correlation-based connectivity approach that has been proposed as an imaging marker for several psychiatric disorders [30]. GFC was calculated in MATLAB using the script of Franzmeier et al. [31], which first applies a threshold of 0.3 and then averages all positive Fisher z-scores of our RSFC maps from the first-level analysis. Note that we followed Cole's approach and included only positive correlation coefficients for computing the GFC, as positive and negative correlations may cancel each other out when averaging the correlation coefficients [31,32]. Finally, to obtain data-driven results, we calculated the Regional Homogeneity (ReHo) in DPARSFA by selecting 27 neighboring voxels both with and without the global signal. ReHo is a voxel-based measure of brain activity, which evaluates the similarity or synchronization between the time series of a given voxel and the nearest neighbors [33]. The ReHo method, as opposed to other data-driven methods, such as ICA, which are well-suited for examining large-scale networks, has been chosen as it does not assume spatial independence of the identified maps and it is not sensitive to region-to-region variability of the hemodynamic response [34]. This has a particular advantage for our study, as it provides an efficient way to assess local synchronization of neural activity, thus offering insights into localized functional connectivity disruptions, which we hypothesize may be impacted in presenilin-1 E280A mutation carriers based on previous findings in the sporadic Alzheimer's disease continuum [35–37]. Indeed, previous studies have suggested that alterations in brain function in Alzheimer's disease, especially in the early stages, may manifest at the local level rather than across widespread, large-scale networks [7,38]. By using ReHo, we maximize the likelihood of detecting these local disruptions, which can complement future studies utilizing techniques like ICA to explore how these initial local changes may eventually contribute to large-scale network dysfunction.

2.5. Amyloid PET analysis

Amyloid PET images were preprocessed using SPM12. Initially, each subject's averaged PET frames were co-registered to their corresponding T1-weighted MRI scan. Then, the co-registered PET images were spatially normalized to the MNI reference template using the deformation parameters derived from the normalization of their corresponding MRI scans.

To extract the florbetapir standard uptake value we used the Centiloid cortical mask and normalized the PET signal to the whole cerebellum Centiloid mask. To define clusters of amyloid positivity, we used the K-means clustering approach [39] implemented in R (R Core Team 2021, version 4.1.0). K-means clustering distinguishes amyloid PET positive from amyloid PET negative by grouping data points based on their similarity in PET scan features. This resulted in two clusters, with a threshold of approximately > 1.12 for amyloid positivity. To visualize the distribution of AV45-PET signal please see Fig. S1.

2.6. Bayesian statistical analysis

We chose Bayesian analysis over a frequentist approach to address the limitations of interpreting p-values, particularly the binary classification of 'significant' versus 'non-significant' results. In frequentist analysis, p-values on opposite sides of 0.05 are often seen as conflicting evidence, which restricts scientific discourse and can lead to erroneous conclusions. The Bayesian framework, in contrast, conceptualizes evidence as a continuum, allowing for direct estimation of support for both the null and alternative hypotheses [40]. This approach provides a nuanced interpretation of our data, avoiding the misconception that studies with p-values near 0.05 inherently conflict and offering a more robust understanding of the evidence. Before starting the analysis, we conducted a Levene's test to determine equality of variances between carriers and non-carriers ($p = 0.250$), thereby justifying the use of parametric testing instead of non-parametric methods (Additional file 2). For GFC and ReHo-based analysis, we used Bayesian Analysis of Covariance (ANCOVA) with Bayes factor (BF) hypothesis testing to compare the null hypothesis against the alternative hypothesis (i.e., the assumption that there is an effect of carrier status, H1) as implemented in Jeffreys's Amazing Statistics Program (JASP, Version 0.16.4), available at jasp-stats.org. We report the BF_{10} quantifying evidence in favor of the alternative hypotheses. Three conclusions are possible within the Bayesian framework: 1) support for the null hypothesis ($BF_{10} < 0.33$); 2) support for the alternative hypothesis ($BF_{10} > 3$); or 3) inconclusive or "anecdotal" evidence ($BF_{10} = 0.33 - 3$) [41]. Additionally, for the support for the alternative hypothesis, we can differentiate distinct levels of evidence: $BF_{10} > 3$ provides "substantial evidence", a BF_{10} above 10 provides "strong evidence", a BF_{10} above 30 provides "very strong evidence" and a BF_{10} above 100 provides "compelling evidence" against the null model. Since the initial ANCOVA analysis produced only inconclusive evidence, we decided to perform post-hoc Bayesian independent informed *t*-tests which allowed us to include our assumptions into the mathematical models. Because *t*-tests do not allow for covariates, we regressed out the covariates' effects using linear regressions and saved the residuals from these regressions [42]. These residuals then served as dependent variables in our post-hoc *t*-tests. These *t*-tests specifically tested the one-sided hypothesis that mutation carriers would have lower functional connectivity in the basal forebrain and hippocampus compared to noncarriers, so mutation status served as the independent variable. To test the hypothesis that carriers have lower connectivity, we truncated the prior distribution at zero, specifying that we expect the posterior distribution to assume exclusively negative values. As we expected the negative effect to be of medium size, we chose a prior Cauchy distribution with a location of −0.707 and a scale of 0.707 [43]. Similarly, we also used Bayesian independent informed *t*-tests to test the hypothesis of lower basal forebrain connectivity in amyloid positive compared to amyloid negative subjects, as well as of reduced ReHo in carriers compared to noncarriers. A more specific description of our statistical models is available in Additional file 2.

3. Results

3.1. Demographics

From the 242 participants of the API ADAD Colombia Trial who underwent resting-state fMRI, we excluded 27 participants due to excessive head motion (FD mean > 0.2) resulting in a final sample size of $N = 215$. Demographic characteristics, cognitive performance and amyloid burden are shown in Table 1. The sample included 147 mutation carriers (mean age: 35 years) and 68 noncarriers (mean age: 40 years). The average years of education was 9. We found compelling evidence in favor of an age difference between groups ($BF_{10} = 5.9 \times 10^6$), with noncarriers being older, but inconclusive evidence for group differences concerning sex, MMSE, CDR scores and education level. We found compelling evidence in favor of a difference in the proportion of amyloid positivity, with only carriers having amyloid positive results ($BF_{10} = 3.581 \times 10^{17}$)(see Table 1 for details). For more details concerning cognitive measures please refer to Supplementary Materials (Table S1).

3.2. Basal forebrain seed-based functional connectivity in carriers and noncarriers

The group-level one sample *t*-test showed connectivity with the anterior and posterior basal forebrain in carriers and noncarriers (Fig. 2 A–D). Regions having connectivity with the anterior basal forebrain were mainly located in the cerebellum, precuneus and posterior medial frontal gyrus bilaterally, as well as in the left middle temporal gyrus and paracentral lobule in carriers ($n = 147$) (Fig. 2 A, Table 2). In noncarriers

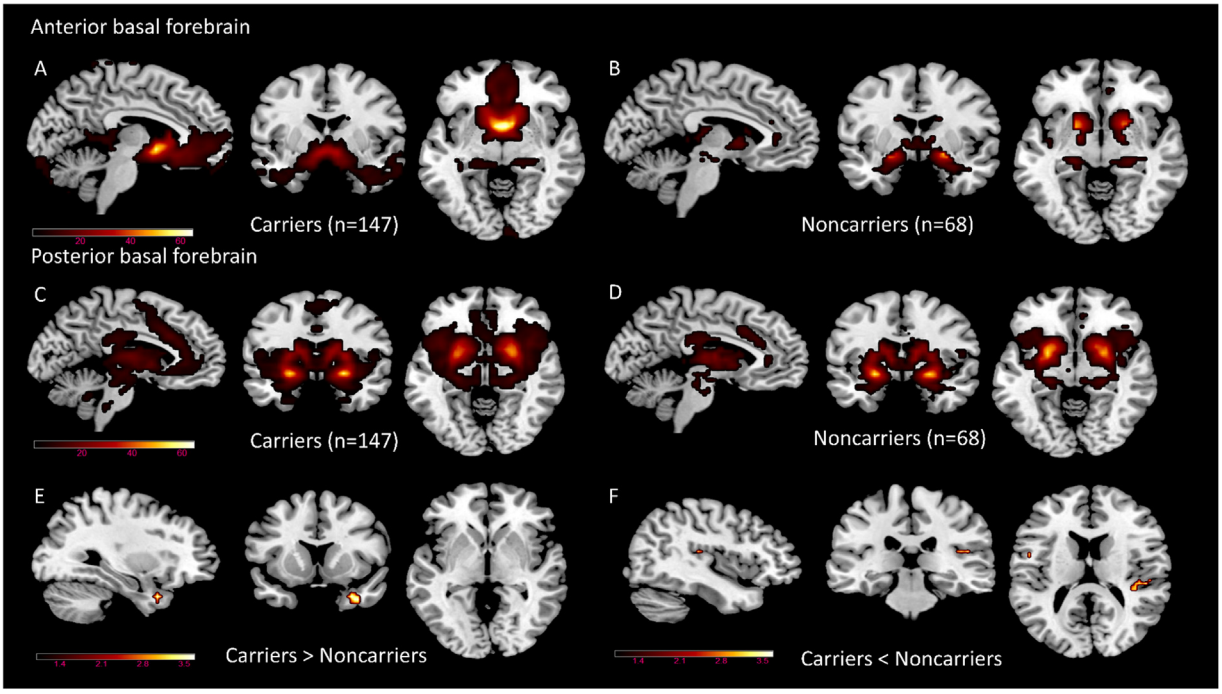

Fig. 2. Functional maps of significant resting-state functional connectivity in basal forebrain. One-sample *t*-tests show the spatial patterns of seed-to-voxel connectivity measures of anterior and posterior basal forebrain subdivisions in **A**), **C**) carriers ($n = 147$) and **B**), **D**) noncarriers ($n = 68$), respectively. T positive values are expressed on a red color scale from 1 to 60 (p value= 0.05 corrected for familywise error at voxel and cluster level). Multiple regressions showing significant differences among groups (contrast 1: carriers > noncarriers, contrast 2: carriers < noncarriers) are represented in figures **E**), **F**). T positive values are expressed on a red color scale from 0 to 4 (p value= 0.01, uncorrected for multiple comparisons). Anterior and posterior basal forebrain seed regions were excluded. Co-variates: age, sex, CDR scores, *APOE* $\varepsilon 4$ and education. Functional images do not include the global signal.

Table 1
Demographic characteristics. Number of subjects, *APOE* $\varepsilon 4$ status, gender, age, education, global cognitive performance, amyloid burden (threshold ≥ 1.12 for amyloid positivity based on AV45 uptake) and memory scores are shown in table. Note: absolute numbers are reported in fractions among the total sample, brackets indicate percentage proportions, otherwise data are provided as means and standard deviations (±). BF = Bayesian Factor, CDR = Clinical Dementia Rating scale, MMSE = Mini-Mental State Examination.

Characteristic	Overall	PSEN1 E280A Carriers	Noncarriers
N. of participants	215	147/215 (68%)	68/215 (32%)
APOE $\varepsilon 4$ carriers	50/215 (23%)	34/147 (23%)	16/68 (23%)
N. of women*	137/215 (64%)	91/147 (62%)	46/68 (68%)
Age (y)†	36.5 ± 6.0	34.8 ± 5.2	40.22 ± 6.2
Education (y)‡	8.8 ± 4.2	8.9 ± 4.1	8.60 ± 4.5
MMSE§	28.9 ± 1.2	28.9 ± 1.3	29.2 ± 0.9
CDR global score¶	0.04 ± 0.1	0.05 ± 0.1	0.04 ± 0.1
Amyloid burden#	85/215 (39%)	85/147 (58%)	0/68 (0%)

* Bayesian contingency table: Bayes factor shows moderate evidence in favor of no difference in proportion of sex between groups ($BF_{10} = 0.251$).

† Bayesian contingency table: Bayes factor Poisson shows compelling evidence in favor of a difference in proportion of age-groups between carriers and noncarriers ($BF_{10} = 5.9 \times 10^6$), with higher age in the noncarriers (50–54 years).

‡ Bayesian contingency table: Bayes factor shows anecdotal evidence in favor of no difference in proportion of years of education between groups ($BF_{10} = 0.377$).

§ Bayesian contingency table: Bayes factor shows moderate evidence in favor of no difference in proportion of CDR global scores between groups ($BF_{10} = 0.197$).

¶ Bayesian Informed *t*-test: Bayes factor shows anecdotal evidence for a difference in CDR score means between groups ($BF_{10} = 1.557$).

Bayesian *t*-test: Bayes factor shows compelling evidence in favor of a difference between groups ($BF_{10} = 3.581 \times 10^{17}$), with noncarriers having no amyloid depositions.

($n = 68$), the anterior basal forebrain was connected with the anterior cingulate cortex (ACC) and medial temporal pole bilaterally, and with the left olfactory cortex, putamen, superior temporal gyrus and temporal pole (Fig. 2 B, Table 2). The posterior basal forebrain showed connections with areas of the cerebellum and middle frontal gyrus bilaterally; with the left putamen, middle frontal gyrus, supramarginal gyrus, postcentral gyrus; and with the right superior-inferior frontal gyri, precentral gyrus and superior medial gyrus in carriers ($n = 147$) (Fig. 2 C, Table 2). In noncarriers ($n = 68$) the posterior basal forebrain showed functional connectivity with the ACC, cerebellum and medial temporal pole bilaterally; with the right insula, putamen, supramarginal gyrus and rolandic operculum (Fig. 2 D, Table 2). Results of the sensitivity analysis including the global signal are reported in the Supplementary Materials (Table S2).

3.3. Effect of carrier status on basal forebrain and hippocampus seed-based functional connectivity and amyloid burden

In the multiple regression model looking at group differences and specifically at carriers with lower connectivity than noncarriers (contrast 2: carriers < noncarriers) and carriers with greater connectivity than noncarriers (contrast 1: carriers > noncarriers), we found a group difference only in the posterior basal forebrain functional connectivity (Table 2). The posterior basal forebrain showed reduced connectivity with the left inferior frontal gyrus, right superior temporal gyrus and right Heschls gyrus, but greater connectivity in the medial temporal pole in carriers compared to noncarriers (Table 2). However, when correcting for multiple comparisons, no supra-threshold clusters survived. For a more complete overview of the locations of functional connectivity including the global signal for the basal forebrain and hippocampus, please refer to Tables S3 and S4 of the Supplementary Materials. In the second multiple regression model with amyloid status as a predictor (contrast: amyloid positive < amyloid negative) within the

Table 2
Location and local functional connectivity for the cholinergic basal forebrain. Upper table reports the results of the one sample *t*-test in carriers (n = 147) and noncarriers (n = 68) separately (p = 0.05, FWE, covariates: age, sex, education, CDR score, and *APOE* ε4). The lower table reports only the significant group differences found for the posterior basal forebrain functional connectivity (p-values < 0.01 uncorrected for multiple comparisons, covariates: age, sex, education, CDR score, *APOE* ε4) between carriers and noncarriers (n = 215). Labels were assigned using the automated anatomical labeling atlas toolbox implemented in SPM12 (http://www.gin.cnrs.fr/AAL). The minimum cluster-size was of 10 voxels. Functional data were regressed for global signal and included basal forebrain network masks. Contrast 1: carriers > noncarriers, contrast 2: carriers < noncarriers, FWE= Family-wise error correction for multiple comparisons.

					MNI coordinate			Significance level
Region label	Cluster-size (voxels)	Region	Side	T	x	y	z	
Anterior basal forebrain network								
Carriers								p = 0.05 (FWE)
	468	Cerebellum (Crus 2)	R	7.244	12	−90	−30	p < 0.001 (FWE)
	10	Cerebellum (Crus 1)	L	5.511	−51	−63	−24	p < 0.001 (FWE)
	21	Middle temporal gyrus	L	6.232	−54	−6	−15	p < 0.001 (FWE)
	38	Precuneus	R	6.219	6	−51	21	p < 0.001 (FWE)
	25	Precuneus	L	5.868	−3	−45	78	p < 0.001 (FWE)
	25	Paracentral lobule	L	5.906	−3	−39	78	p < 0.001 (FWE)
	16	Posterior-medial frontal	L	5.782	0	−6	78	p < 0.001 (FWE)
	16	Posterior-medial frontal	R	5.444	3	−18	78	p < 0.001 (FWE)
Noncarriers								
	1045	Olfactory cortex	L	31.729	−21	3	−9	p < 0.001 (FWE)
	1045	Putamen	L	28.446	−21	12	−3	p < 0.001 (FWE)
	117	Anterior cingulate cortex	L	8.739	0	30	21	p < 0.001 (FWE)
	117	Anterior cingulate cortex	R	8.643	3	36	6	p < 0.001 (FWE)
	15	Superior temporal gyrus	L	6.999	−42	−18	3	p < 0.001 (FWE)
	30	Medial temporal pole	R	6.958	36	21	−30	p < 0.001 (FWE)
	21	Medial temporal pole	L	6.646	−39	15	−30	p < 0.001 (FWE)
	13	Temporal pole	L	5.956	−45	12	−12	p < 0.001 (FWE)
Posterior basal forebrain network								
Carriers								
	8404	Putamen	L	32.120	−24	6	6	p < 0.001 (FWE)
	74	Cerebellum (VI)	R	8.237	33	−51	−27	p < 0.001 (FWE)
	75	Cerebellar Vermis (9)		8.128	0	−51	−33	p < 0.001 (FWE)
	75	Cerebellum	L	6.504	−9	−51	−33	p < 0.001 (FWE)
	75	Cerebellum (IX)	R	6.072	12	−54	−33	p < 0.001 (FWE)
	95	Cerebellum (VI)	L	6.689	−21	−60	−21	p < 0.001 (FWE)
	10	Cerebellum (VIII)	L	6.051	−27	−57	−48	p < 0.001 (FWE)
	13	Precentral gyrus	R	7.879	54	3	48	p < 0.001 (FWE)
	72	Inferior frontal gyrus	R	8.267	48	42	3	p < 0.001 (FWE)
	72	Middle frontal gyrus	R	6.151	48	51	9	p < 0.001 (FWE)
	105	Middle frontal gyrus	L	6.689	−21	−60	−21	p < 0.001 (FWE)
	44	Middle frontal gyrus	R	5.640	30	48	21	p < 0.001 (FWE)
	65	Postcentral gyrus	L	6.903	−60	−24	27	p < 0.001 (FWE)
	65	Supramarginal gyrus	L	5.738	−54	−33	30	p < 0.001 (FWE)
	44	Superior frontal gyrus	R	6.264	33	57	24	p < 0.001 (FWE)
	20	Superior medial gyrus	R	5.911	15	60	36	p < 0.001 (FWE)
Noncarriers								
	4098	Putamen	R	25.947	21	9	−3	p < 0.001 (FWE)
	435	Anterior cingulate cortex	R	9.191	3	27	24	p < 0.001 (FWE)
	435	Anterior cingulate cortex	L	9.032	−9	18	36	p < 0.001 (FWE)
	22	Insula lobe	R	7.955	42	−21	9	p < 0.001 (FWE)
	21	Supramarginal gyrus	R	5.646	63	−33	33	p < 0.001 (FWE)
	10	Rolandic operculum	R	5.536	54	0	12	p < 0.001 (FWE)
	67	Cerebellum (VI)	L	7.695	−30	−57	−27	p < 0.001 (FWE)
	63	Cerebellum (VI)	R	6.927	33	−54	−27	p < 0.001 (FWE)
	10	Cerebellar Vermis (4/5)		6.555	0	−54	3	p < 0.001 (FWE)
	20	Medial temporal lobe	L	6.648	−39	15	−30	p < 0.001 (FWE)
	33	Medial temporal lobe	R	6.959	36	21	−30	p < 0.001 (FWE)
Posterior basal forebrain network								
Contrast 1: carriers > noncarriers								p = 0.01 (uncorr.)
	18	Medial temporal pole	R	3.617	30	12	−33	p < 0.01 (uncorr.)
Contrast 2: carriers < noncarriers								
	12	Inferior frontal gyrus	L	3.325	−51	0	12	p < 0.01 (uncorr.)
	11	Superior temporal gyrus	R	3.217	48	−27	15	p < 0.01 (uncorr.)
	11	Heschls gyrus	R	3.117	42	−27	15	p < 0.01 (uncorr.)

carriers group only (n = 147), we found reduced connectivity of anterior basal forebrain with the right inferior frontal gyrus, fusiform gyrus, parahippocampal gyrus, left inferior temporal gyrus, lingual gyrus. We also found reduced connectivity of the posterior basal forebrain with the parahippocampal gyrus, middle temporal gyrus, hippocampus and left fusiform gyrus (p < 0.01, uncorrected). Yet, none of these clusters survived multiple comparison corrections (Fig. S2).

The ANCOVA revealed inconclusive to moderate evidence against an effect of mutation status on the seed-based global functional connectivity of basal forebrain and hippocampus (GFC anterior basal forebrain: BF_{10} = 0.97; GFC posterior basal forebrain: BF_{10} = 0.487; GFC left hippocampus: BF_{10} = 0.187; GFC right hippocampus: BF_{10} = 0.157). Subsequently, the post-hoc Bayesian independent informed *t*-tests yielded anecdotal to strong evidence against an effect of carrier status on an-

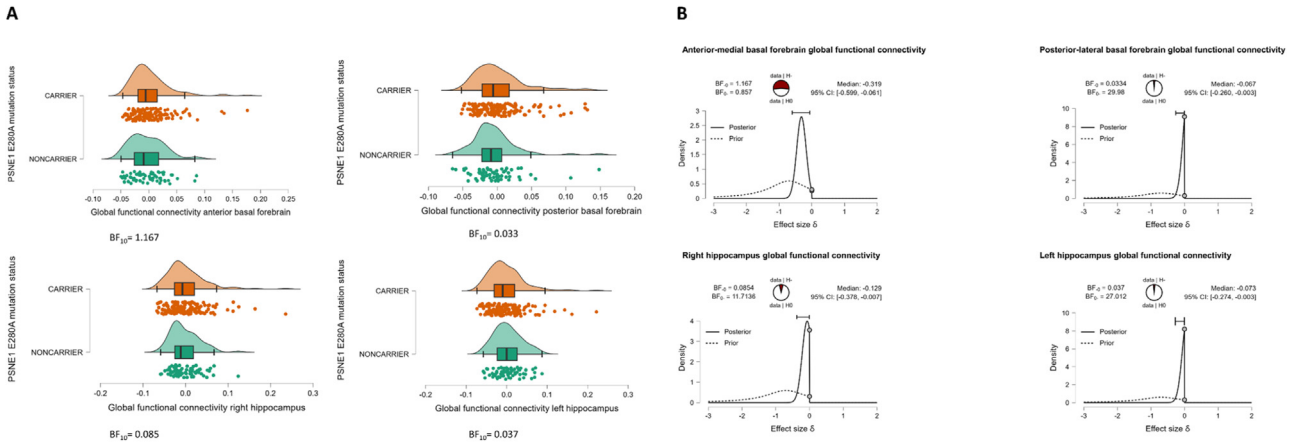

Fig. 3. Effect of mutation status on basal forebrain and hippocampus functional connectivity. **A**) depicts raincloud plots of Bayesian independent informed *t*-tests results testing the one-sided alternative hypothesis that the population mean of the group carrier is smaller than the population mean of the noncarriers group. X-axis depicts the mean of basal forebrain global functional connectivity. Residuals of age, sex, education, *APOE* ε4 and CDR were regressed out on basal forebrain global functional connectivity measures. BF = Bayes Factor (BF = 0.33 – 3 is considered inconclusive or anecdotal evidence, BF > 3 is considered moderate evidence, BF > 10 is considered strong evidence). Global functional connectivity values do not include the global signal. **B**) shows Bayesian independent informed one-tailed *t*-tests with subjective priors and posteriors. Plots show the mismatch between our prior expectation (alternative hypothesis) and the posterior observation (outcome variable). The probability wheel on top visualizes the evidence that the data provide for the two rival hypotheses. The posterior distribution is much more peaked than the prior distribution, indicating that our data have been highly informative, so that these analyses provide a high degree of certainty that in these data, the effect size is centered on zero, and has aggregated there over all sampling. Note: for all tests, the alternative hypothesis specifies that the location of group "carriers" is smaller than the location of group "noncarriers" (one-direction hypothesis). The two gray dots indicate the prior and posterior density at the test value. The median and the 95% central credible interval of the posterior distribution are shown in the top right corner. BF = Bayes Factor. Global functional connectivity values do not include the global signal.

terior basal forebrain (BF_{10} = 1.167), posterior basal forebrain (BF_{10} = 0.033), as well as moderate to strong evidence against an effect of carrier status on right hippocampus (BF_{10} = 0.085) and left hippocampus (BF_{10} = 0.037) global positive functional connectivity (Fig. 3 A). These results indicate that we ought to reject the hypotheses under consideration. To observe the mismatch between the priori hypothesis and the null model please refer to Fig. 3 B. Similarly, Bayesian independent informed *t*-tests testing the one-sided hypothesis that the population mean of the carrier group is smaller than the population mean of the noncarriers group, showed very strong to strong evidence that amyloid status has no effect on anterior (BF_{10} = 0.040) or posterior (BF_{10} = 0.025) basal forebrain and moderate evidence that amyloid status's effect is also absent in the hippocampus (left hippocampus: BF_{10} = 0.037; right hippocampus: BF_{10} = 0.036) global functional connectivity. For the sensitivity analysis, Table S5 shows the effects of carrier status on the basal forebrain and hippocampus.

3.4. Data-driven results

ReHo analysis showed reduced signal in the cerebellar vermis (t-value=3.226; p < 0–0.01 uncorrected), left cerebellum (t-value=3.109; p < 0–0.01 uncorrected) and postcentral gyrus (t-value=2.891; p < 0–0.01 uncorrected), as well as right inferior frontal gyrus (t-value=3.223; p < 0.01 uncorrected) in mutation carriers compared to noncarriers. In contrast, carriers showed increased ReHo signal in the left middle temporal gyrus (t-value=3.943; p < 0.01 uncorrected), cerebellum (bilateral) (t-values=2.548–3.471; p < 0.01 uncorrected), left rectal gyrus (t-value=3.097; p < 0.01 uncorrected), left superior orbital gyrus (t-value=2.756; p < 0.01 uncorrected). For ReHo analysis including the global signal, please see Table S6. Bayesian ANCOVA results revealed compelling evidence of reduced functional connectivity in carriers compared to noncarriers in the clusters identified using the ReHo method (cluster 1 Cerebellum: BF_{10}= 276; cluster 2 left postcentral gyrus: BF_{10} =199; cluster 3 right inferior frontal gyrus: BF_{10} = 259.718). Similarly, Bayesian ANCOVA showed compelling evidence of increased functional connectivity in carriers compared to noncarriers in the clusters identified by ReHo (cluster 1 right Cerebellum (crus1): BF_{10} = 1831.245; cluster 2 left Cerebellum (crus2): BF_{10} = 289.698; cluster 3 left rectal gyrus and superior orbital gyrus: BF_{10} = 586.939; cluster 4 left middle temporal gyrus: BF_{10} = 292.255; cluster 5 right Cerebellum (crus 1): BF_{10} = 121; cluster 6 left Cerebellum (crus 1): BF_{10} = 194.369) (Table S7). However, post-hoc Bayesian independent informed *t*-tests found compelling evidence only in favor of reduced cerebellar connectivity (BF_{10} = 96.67, δ = 0.5, 95% CI: [0.211 – 0.796]), as well as in favor of reduced connectivity of the right inferior frontal gyrus (BF_{10} = 145, δ = 0.521, 95% CI: [0.228–0.815]) and of the left post-central gyrus (BF_{10} = 158, δ = 0.525, 95 % CI: [0.2[– 0.819]) in carriers compared to noncarriers. For the sensitivity analysis, Table S5 shows also results from Bayesian independent informed *t*-tests.

4. Discussion

The current study aimed at assessing basal forebrain functional connectivity and its association with amyloid load in the baseline data of asymptomatic *PSEN1 E280A* mutation carriers compared with noncarriers from the API ADAD Trial [20]. Contrary to our primary hypothesis, we found evidence against a reduction of basal forebrain and hippocampal functional connectivity in carriers compared to noncarriers. These results disagree with results in sporadic prodromal and preclinical AD cases [7]. Moreover, in the Alzheimer's Disease Neuroimaging Initiative (ADNI) cohort, lower basal forebrain functional connectivity has been found in MCI/AD individuals with abnormal versus normal CSF in the nucleus basalis of Meynert [44]. In contrast with our second hypothesis, we found moderate to very strong evidence against an association of basal forebrain and hippocampus functional connectivity with amyloid pathology in mutation carriers. This differs from a study on sporadic AD that found reduced basal forebrain connectivity in association with amyloid positivity in people with subjective cognitive complaints [6]. This is also in contrast with a study showing functional alterations of the hippocampus during encoding of novel face-name pairs in twenty asymptomatic Colombian *PSEN1* mutation carriers compared to nineteen noncarriers of the same kindred [19]. The lack of a reduction in basal forebrain connectivity may be explained by evidence from transgenic mouse models. Abnormal sprouting or redistribution of choliner-

gic processes may occur in response to amyloid deposition. In *PSEN1* or APP transgenic mice, amyloid pathology enhances the cholinergic phenotype, including abnormal sprouting and redistribution of cholinergic processes in the cortex. This may also occur in humans, obscuring expected reductions in connectivity [45].

Nonetheless, our results are partly in line with a study from the Dominantly Inherited Alzheimer Network (DIAN) cohort showing that brain global functional connectivity was reduced in mutation carriers with CDR scores greater than 0 (impaired), but not in mutation carriers with CDR scores equal to 0 (cognitively normal) compared to noncarriers [46]. Also, previous studies showed that basal forebrain volume is reduced in preclinical and prodromal AD individuals with tau pathology, but not in individuals with Aβ pathology [47] and that, higher concentrations of plasma t-tau are associated with higher rates of atrophy in the basal forebrain [48]. Likewise, Strain and colleagues found no reliable abnormalities in both brain covariance and correlation functional connectivity at CDR <1 in the two cohorts of ADAD and sporadic Late-Onset Alzheimer's Disease (LOAD) [49]. The basal forebrain has not been studied before in familial AD and not by using neuroimaging markers like resting-state functional connectivity. Preclinical studies on changes in the cholinergic system presented controversial results [50,51]. A study using PS1/A246E transgenic mice as a model of ADAD found hypermetabolic activity in the basal forebrain, which was thought to represent a compensatory response to mitochondrial abnormalities [51]. A review reported that studies using human stem cells found a reduction in neuronal excitability in cholinergic basal forebrain neurons, but for another kind of mutation (*PSEN2* N141I) [50].

Our findings generate the new hypothesis that, in resting-state conditions, the cholinergic basal forebrain is functionally preserved in asymptomatic *PSEN1 E280A* mutation carriers. A previous study from the same sample [52] found no evidence of basal forebrain and hippocampus atrophy and no association with amyloid load, but rather a relative preservation of basal forebrain metabolism in mutation carriers. Together, these data provide new evidence for familial versus sporadic forms of Alzheimer's disease. A possible explanation for the assumption of global basal forebrain preservation in mutation carriers may be connected to age as a factor of brain resilience. Indeed, the carriers' mean age was 35 years, five years lower than in noncarriers (40 years). Previous studies on this population showed that the median age of onset is 44 years. Therefore, our analysis captured cases of mutation carriers presumably on average nine years before the emergence of clinical symptoms [10], even though we found no association between basal forebrain global connectivity and age within this group. A study on resting-state fMRI in familial AD has demonstrated that brain global functional connectivity varies non-linearly concerning estimated years of symptoms onset (EYO), with an initial increase early in the disease time course (EYO = 17 years) followed by a period of stabilization until further decreasing close to the estimated time of disease manifestation (EYO = 0.5 years) [46]. This may be an indication that the subjects in our sample are in a phase of either a relative increase in functional connectivity or a plateau. Surely, the interaction between demographic, genetic, neurofunctional, cognitive reserve and occupational factors in this population needs to be further investigated [22], especially in light of recently reported single cases of extreme resilience to ADAD [53]. In that report, two siblings carrying the RELN–COLBOS and *PSEN1 E280A* genes showed a delayed disease manifestation relative to their estimated age of disease onset. However, the female sibling exhibited faster decline and more severe disease progression than her brother, likely due to depression and other comorbidities [53]. To this extent, future studies should investigate the relationship between indices of cholinergic functional connectivity and AD biomarkers, as well as psychiatric conditions especially depression [22,53], which is common in this population.

Our data-driven results revealed a notable discrepancy in the ReHo signal, with opposing trends observed in different brain regions. However, only the cerebellum exhibited a statistically significant reduction in the ReHo signal between carriers and non-carriers. In general, the ReHo results indicating increased connectivity in asymptomatic PSEN1 mutation carriers compared to non-carriers may be indicative of compensatory mechanisms, whereas decreased connectivity could suggest aberrant connectivity [38]. These findings are consistent with those of a study on sporadic AD that correlated ReHo patterns in the temporal, parietal, and frontal regions with cognitive testing outcomes in individuals with SCD and MCI compared to healthy controls [38]. This study demonstrated a correlation between decreased ReHo and poorer performance on cognitive testing, as well as a correlation between increased ReHo and better performance on cognitive testing [38]. Nonetheless, little research has been conducted on the connectivity of the cerebellum in sporadic AD and ADAD [54]. A recent study in sporadic AD patients has shown that decreased connectivity between the cerebellum and thalamus may disrupt the cerebellum's connectivity with other cognitive networks like the Default Mode Network, resulting in cognitive impairment [54]. Similarly, one PET study conducted in the API ADAD Colombia Trial and Colombia-Boston cohorts showed greater evidence of cerebellar amyloid plaque deposition in carriers, already 10 years before the estimated age of MCI onset [55]. Lastly, a case report comparing an advanced-stage APP Osaka mutation patient with early-onset sporadic AD patients and healthy subjects revealed high tau accumulation but subtle Aβ burden in the cerebral cortex, most pronounced in the cerebellum, suggesting that tau accumulation may be a potential marker for the distinction of familial from sporadic AD [56].

This study has some limitations. Firstly, these are baseline cross-sectional data. Secondly, based on the data we received, we could not calculate the exact EYO in mutation carriers [22]. Additionally, besides education, no data on occupational attainment were collected at baseline to measure variables such as cognitive reserve that could explain protective or neuroplasticity mechanisms [22]. Also, no data on neuropsychiatric scales measuring depression or other comorbidities were accessible to us. Future studies should replicate our results in different ADAD cohorts. It would be important to determine if and how cholinergic functional connectivity changes over time, as well as its relationship with other cognitive indices, age of disease onset and AD biomarkers.

To conclude, our study showing the functional preservation of the cholinergic basal forebrain and hippocampus but the disruption of ReHo cerebellar signal in asymptomatic mutation carriers, despite falsifying our original hypothesis, enriches the evidence on the neuropathological processes of ADAD. Nonetheless, the insensitivity of the ReHo method to shape differences between clusters is a common drawback; therefore, results obtained from data-driven analysis should be interpreted cautiously, especially considering the type, spatial distribution, and distance of the anatomical regions involved. Replication of such findings using other data-driven methods (e.g., ICA) will be considered in future studies to complement our findings. Finally, these findings may have important implications, suggesting potential new avenues for pharmaceutical interventions. If these results are replicated, other brain regions or proteins, such as the cerebellum and tau, may offer novel treatment targets for familial AD. This is particularly relevant, as recent clinical trials in this population targeting amyloid accumulation have failed to demonstrate significant benefits [57,58].

Declaration of generative AI and AI-assisted technologies in the writing process

During the preparation of this work the authors used DeepL Write and Grammarly in order to improve the readability and language of the manuscript. After using these tools, the authors reviewed and edited the content as needed and take full responsibility for the content of the published article.

Declaration of competing interest

Stefan J. Teipel reports being Advisory Board Member at Lilly, Eisai, Biogen, and GE Healthcare. Martin Dyrba reports grants from the Ger-

man Research Foundation (DFG) outside the submitted work. All the other authors have no conflict of interest.

CRediT authorship contribution statement

Alice Grazia: Writing – review & editing, Writing – original draft, Visualization, Software, Methodology, Formal analysis, Conceptualization. **Martin Dyrba:** Writing – review & editing, Software, Methodology, Data curation. **Nunzio Pomara:** Writing – review & editing, Conceptualization. **Anna G. Temp:** Writing – review & editing, Methodology. **Michel J. Grothe:** Writing – review & editing. **Stefan J. Teipel:** Writing – review & editing, Supervision, Resources, Project administration, Data curation, Conceptualization.

Funding

Open Access funding enabled and organized by Project DEAL. This publication was made possible by the API ADAD Trial related grants RF1AG041705, R01AG055444, P30AG072980 from the National Institute of Health (NIH) and National Institute of Aging (NIA). The API ADAD Trial was also supported by the NIA grants, Genentech and its parent organization Roche, and generous philanthropic contributions to the Banner Alzheimer's Foundation. The API ADAD Trial and its related programs have been supported by Banner Alzheimer's Foundation, NOMIS Foundation, FIL/Fidelity Bermuda Foundation, Flinn Foundation and Colciencias.

Acknowledgments

The authors acknowledge the contributions of the Alzheimer's Prevention Initiative (API) team and its collaborators (more information available at https://alzheimerspreventioninitiative.com). They also acknowledge the generous support for the API ADAD trial from grants RF1AG041705 and R01 AG055444 from the National Institute on Aging, grants from Colciencias, grants from the Arizona Alzheimer's Consortium, collaborative research agreements with Genentech and its parent organization Roche; philanthropic support from Banner Alzheimer's Foundation, FIL/Fidelity Bermuda Foundation, Flinn Foundation, Forget Me Not Initiative, and the NOMIS Foundation. The contents of this paper are solely the responsibility of the authors and do not necessarily represent the official views of the funders or partners. The authors would like to thank their valued research participants and families, current and former colleagues in the API ADAD Trial, and the collaborators from DIAN, the A4 Trials Program and CAP for exchanging information about policies and procedures to share data and samples in ways that provide appropriate participant and trial protections. The Alzheimer's Prevention Initiative website hosts materials and details regarding the API ADAD Trial and data sharing process for review or download at https://alzheimerspreventioninitiative.com.

Supplementary materials

Supplementary material associated with this article can be found, in the online version, at doi:10.1016/j.tjpad.2024.100030.

References

[1] Bohnen NI, Grothe MJ, Ray NJ, Müller MLTM, Teipel SJ. Recent advances in cholinergic imaging and cognitive decline-Revisiting the cholinergic hypothesis of dementia. Curr Geriatr Rep 2018;7(1):1–11 PMID: 29503795. doi:10.1007/s13670-018-0234-4.

[2] Mesulam MM. Chapter 28 The systems-level organization of cholinergic innervation in the human cerebral cortex and its alterations in Alzheimer's disease. Prog Brain Res 1996;109:285–97. doi:10.1016/S0079-6123(08)62112-3.

[3] Groethe M, Heinsen H, Teipel S. Atrophy of the Cholinergic Basal Forebrain Over the Adult Age Range and in Early Stages of Alzheimer's Disease. Biol. Psychiatry 2012;71(9). doi:10.1016/j.biopsych.2011.06.019.

[4] Schmitz TW, Nathan Spreng R. Basal forebrain degeneration precedes and predicts the cortical spread of Alzheimer's pathology. Nat Commun 2016;7:13249 PMID: 27811848. doi:10.1038/ncomms13249.

[5] Fritz H-CJ, Ray N, Dyrba M, Sorg C, Teipel S, Grothe MJ. The corticotopic organization of the human basal forebrain as revealed by regionally selective functional connectivity profiles. Hum Brain Mapp 2018;40(3):868–78 PMID: 30311315. doi:10.1002/hbm.24417.

[6] Herdick M, Dyrba M, Fritz HCJ, et al. Multimodal MRI analysis of basal forebrain structure and function across the Alzheimer's disease spectrum. NeuroImage: Clinical 2020;28. doi:10.1016/j.nicl.2020.102495.

[7] Chiesa PA, Cavedo E, Groethe M, et al. Relationship between basal forebrain resting-state functional connectivity and brain amyloid-b deposition in cognitively intact older adults with subjective memory complaints. Radiology 2019;290:167–76. doi:10.1148/radiol.2018180268.

[8] Bateman RJ, Aisen PS, Strooper B de, et al. Autosomal-dominant Alzheimer's disease: a review and proposal for the prevention of Alzheimer's disease. Alzheimer Res Ther 2011;3(1). doi:10.1186/alzrt59.

[9] Cornejo W, Lopera F, Uribe CS, Salinas M. Descripcion de una familia con demencia presenil tipo Alzheimer /Description of a family with presenile dementia type Alzheimer. Acta Médica Colombiana 1987;12(2).

[10] Acosta-Baena N, Sepulveda-Falla D, Lopera-Gómez CM, et al. Pre-dementia clinical stages in presenilin 1 E280A familial early-onset Alzheimer's disease: a retrospective cohort study. Lancet Neurol 2011;10. doi:10.1016/S1474-4422(10)70323-9.

[11] Tariot PN, Lopera F, Langbaum JB, et al. The Alzheimer's Prevention Initiative Autosomal-Dominant Alzheimer's Disease Trial: a study of crenezumab versus placebo in preclinical PSEN1 E280A mutation carriers to evaluate efficacy and safety in the treatment of autosomal-dominant Alzheimer's disease, including a placebo-treated noncarrier cohort. Alzheimer Dement (N Y) 2018;4:150–60 PMID: 29955659. doi:10.1016/j.trci.2018.02.002.

[12] Fleisher AS, Chen K, Quiroz YT, et al. Florbetapir PET analysis of amyloid-β deposition in the presenilin 1 E280A autosomal dominant Alzheimer's disease kindred: a cross-sectional study. Lancet Neurol 2013;11(12):70227 -2. doi:10.1016/S1474-4422(12)70227-2.

[13] Aguirre-Acevedo D, Gomez R, Heano-Arboleda E, et al. Validity and reliability of the CERAD-Col neuropsychological battery. Rev Neurol 2007;45(11):655–60.

[14] Qiu Q. Neural networks in autosomal dominant Alzheimer's disease: insights from functional magnetic resonance imaging studies. Front Aging (Albany NY) Neurosci 2022;14. doi:10.3389/fnagi.2022.903269.

[15] Chhatwal JP, Schultz AP, Johnson K, et al. Impaired default network functional connectivity in autosomal dominant Alzheimer disease. Neurology 2013;81(8):736–44. doi:10.1212/WNL.0b013e3182a1aafe.

[16] Zhao T, Quan M, Jia J. Functional connectivity of default mode network subsystems in the presymptomatic stage of autosomal dominant Alzheimer's disease. J Alzheimer Dis 2020;73(4):1435–44 PMID: 31929167. doi:10.3233/JAD-191065.

[17] Quan M, Zhao T, Tang Y, et al. Effects of gene mutation and disease progression on representative neural circuits in familial Alzheimer's disease. Alzheimer Res Ther 2020;12(1):14 PMID: 31937364. doi:10.1186/s13195-019-0572-2.

[18] Fleisher AS, Chen K, Quiroz YT, et al. Associations between biomarkers and age in the presenilin 1 E280A autosomal dominant Alzheimer disease kindred: a cross-sectional study. JAMA Neurol 2015;72(3):316–24 PMID: 25580592. doi:10.1001/jamaneurol.2014.3314.

[19] Quiroz YT, Budson AE, Celone K, et al. Hippocampal hyperactivation in presymptomatic familial Alzheimer's disease. Ann Neurol 2010;68(6):865–75 PMID: 21194156. doi:10.1002/ana.22105.

[20] Reiman EM, Pruzin JJ, Rios-Romenets S, et al. A public resource of baseline data from the Alzheimer's Prevention Initiative Autosomal-Dominant Alzheimer's Disease Trial. Alzheimer Dement 2022;19:1938–46. doi:10.1002/alz.12843.

[21] Lendon CL, Martinez, Alonso, Martinez, Behrens IM, et al. E280A PS-1 mutation causes Alzheimer's disease but age of onset is not modified by ApoE alleles. Hum Mutat 1997;10:186–95. doi:10.1002/(SICI)1098-1004(1997)10:3<186::AID-HUMU2>3.0.CO;2-H.

[22] Rios-Romenets S, Lopera F, Sink KM, et al. Baseline demographic, clinical, and cognitive characteristics of the Alzheimer's Prevention Initiative (API) Autosomal-Dominant Alzheimer's Disease Colombia Trial. Alzheimer Dement 2020;16:1023–30. doi:10.1002/alz.12109.

[23] Friston KJ, Williams S, Howard R, Frackowiak, Richard SJ, Turner R. Movement-related effects in fMRI time-series. Magn Reson Med 1996;35(3). doi:10.1002/mrm.1910350312.

[24] Golestani M, Jean Chen. Comparing data-driven physiological denoising approaches for resting-state fMRI: implications for the study of aging. Front (Boulder) Front Neurosci 2024;18. doi:10.3389/fnins.2024.1223230.

[25] Agrawal U, Brown EN, Lewis LD. Model-based physiological noise removal in fast fMRI. Neuroimage 2020;205:116231 PMID: 31589991. doi:10.1016/j.neuroimage.2019.116231.

[26] Aquino KM, Fulcher BD, Parkes L, Sabaroedin K, Fornito A. Identifying and removing widespread signal deflections from fMRI data: rethinking the global signal regression problem. Neuroimage 2020;212:116614 PMID: 32084564. doi:10.1016/j.neuroimage.2020.116614.

[27] Liu TT, Nalci A, Falahpour M. The global signal in fMRI: nuisance or Information? Neuroimage 2017;150:213–29 PMID: 28213118. doi:10.1016/j.neuroimage.2017.02.036.

[28] Jenkinson M, et al. Improved optimization for the robust and accurate linear registration and motion correction of brain images. Neuroimage 2002;17:825–41. doi:10.1006/nimg.2002.1132.

[29] Power JD, Barnes KA, Snyder AZ, Schlaggar BL, Petersen SE. Spurious but systematic correlations in functional connectivity MRI networks arise from subject motion. Neuroimage 2012;59(3):2142–54 PMID: 22019881. doi:10.1016/j.neuroimage.2011.10.018.

[30] Kraus C, Mkrtchian A, Kadriu B, Nugent AC, Zarate CA, Evans JW. Evaluating global brain connectivity as an imaging marker for depression: influence of preprocessing strategies and placebo-controlled ketamine treatment. Neuropsychopharmacology 2020;45(6):982–9 PMID: 31995812. doi:10.1038/s41386-020-0624-0.
[31] Franzmeier N, Caballero MÁA, Taylor ANW, et al. Resting-state global functional connectivity as a biomarker of cognitive reserve in mild cognitive impairment. Brain Imaging Behav 2017;11(2):368–82 PMID: 27709513. doi:10.1007/s11682-016-9599-1.
[32] Cole MW, Yarkoni T, Repovs G, Anticevic A, Braver TS. Global connectivity of prefrontal cortex predicts cognitive control and intelligence. J Neurosci 2012;32(26):8988–99 PMID: 22745498. doi:10.1523/JNEUROSCI.0536-12.2012.
[33] Zang Y, Jiang T, Lu Y, He Y, Tian L. Regional homogeneity approach to fMRI data analysis. Neuroimage 2003;20(4):1903–2364. doi:10.1016/j.neuroimage.2003.12.030.
[34] Cole DM, Smith SM, Beckmann CF. Advances and pitfalls in the analysis and interpretation of resting-state FMRI data. Front Syst Neurosci 2010;4. doi:10.3389/fnsys.2010.00008.
[35] Cai S, Jiang Y, Wang Y, et al. Modulation on brain gray matter activity and white matter integrity by APOE ε4 risk gene in cognitively intact elderly: a multimodal neuroimaging study. Behav Brain Res 2017;322:100–9 Pt APMID: 28108320. doi:10.1016/j.bbr.2017.01.027.
[36] Wang Y, Zhao X, Xu S, et al. Using regional homogeneity to reveal altered spontaneous activity in patients with mild cognitive impairment. Biomed Res Int 2015. doi:10.1155/2015/807093.
[37] Zhang Z, Liu Y, Jiang T, et al. Altered spontaneous activity in Alzheimer's disease and mild cognitive impairment revealed by Regional Homogeneity. Neuroimage 2012;59(2):1429–40 PMID: 21907292. doi:10.1016/j.neuroimage.2011.08.049.
[38] Zhang Z, Cui L, Huang Y, Li Y, Guo Q. Changes of regional neural activity homogeneity in preclinical Alzheimer's disease: compensation and dysfunction. Front Neurosci 2021:15. doi:10.3389/fnins.2021.646414.
[39] MacQueen J. Some methods for classification and analysis of multivariate observations. In: Proceedings of 5-th Berkeley Symposium on Mathematical Statistics and Probability. University of California Press; 1967.
[40] Temp AGM, Lutz MW, Tang Y, Wagenmakers E-J, Khachaturian AS, Teipel S. How Bayesian statistics may help answer some of the controversial questions in clinical research on Alzheimer's disease. Alzheimer Dement 2021;17:917–19. doi:10.1002/alz.12374.
[41] Wagenmakers E-J, Marsman M, Jamil T, et al. Bayesian inference for psychology. Part I: theoretical advantages and practical ramifications. Psychon Bull Rev 2018;25(1):35–57 PMID: 28779455. doi:10.3758/s13423-017-1343-3.
[42] Terza JV, Basu A, Rathouz PJ. Two-stage residual inclusion estimation: addressing endogeneity in health econometric modeling. J Health N Hav Econ. 2008;27:531–43. doi:10.1016/j.jhealeco.2007.09.009.
[43] van Doorn J, van den Bergh D, Böhm U, et al. The JASP guidelines for conducting and reporting a Bayesian analysis. Psychon Bull Rev 2021;28:813–26. doi:10.3758/s13423-020-01798-5.
[44] Mieling M, Göttlich M, Yousuf M, Bunzeck N. for the Alzheimer's Disease Neuroimaging Initiative. Basal forebrain activity predicts functional degeneration in the entorhinal cortex in Alzheimer's disease. Brain commun 2023;5(5). doi:10.1093/braincomms/fcad262.
[45] Hernandez D, Sugaya K, Qu T, McGowan E, Duff K, McKinney M. Survival and plasticity of basal forebrain cholinergic systems in mice transgenic for presenilin-1 and amyloid precursor protein mutant genes. Neuroreport 2001;12(7). doi:10.1097/00001756-200105250-00018.
[46] Smith RX, et al. Resting-state functional connectivity disruption as a pathological biomarker in autosomal dominant Alzheimer disease. Brain Connect 2021;11(3). doi:10.1089/brain.2020.0808.
[47] Cavedo E, Lista S, Houot M, et al. Plasma tau correlates with basal forebrain atrophy rates in people at risk for Alzheimer disease. Neurology 2020;94(1):e30–41 PMID: 31801830. doi:10.1212/WNL.0000000000008696.
[48] Cantero JL, Atienza M, Lage C, et al. Atrophy of basal forebrain initiates with tau pathology in individuals at risk for Alzheimer's disease. Cereb Cortex 2020;30(4):2083–98 PMID: 31799623. doi:10.1093/cercor/bhz224.
[49] Strain JF, Brier MR, Tanenbaum A, et al. Covariance-based vs. correlation-based functional connectivity dissociates healthy aging from Alzheimer disease. Neuroimage 2022;261:119511 PMID: 35914670. doi:10.1016/j.neuroimage.2022.119511.
[50] Trombetta-Lima M, Sabogal-Guáqueta AM, Dolga AM. Mitochondrial dysfunction in neurodegenerative diseases: a focus on iPSC-derived neuronal models. Cell Calc 2021;94:102362 PMID: 33540322. doi:10.1016/j.ceca.2021.102362.
[51] Strazielle C, Jazi R, Verdier Y, Qian S, Lalonde R. Regional brain metabolism with cytochrome c oxidase histochemistry in a PS1/A246E mouse model of autosomal dominant Alzheimer's disease: correlations with behavior and oxidative stress. Neurochem Int 2009;55:806–14. doi:10.1016/j.neuint.2009.08.005.
[52] Teipel S, Grazia A, Dyrba M, Groethe M, Pomara N. Basal forebrain volume and metabolism in carriers of the Colombian mutation for autosomal dominant Alzheimer's disease. Sci Rep 2024;14(11268). doi:10.1038/s41598-024-60799-9.
[53] Lopera F, Claudia M, Anita SC, et al. Resilience to autosomal dominant Alzheimer's disease in a Reelin-COLBOS heterozygous man. Nat Med 2023;29. doi:10.1038/s41591-023-02318-3.
[54] Fanyu T, Donglin Z, Wenying M, Qun Y, Qian L, Jingping S. Differences changes in cerebellar functional connectivity between mild cognitive impairment and alzheimer's disease: a seed-based approach. Front Neurol 2021;12. doi:10.3389/fneur.2021.645171.
[55] Ghisays V, Lopera F, Goradia DD, et al. PET evidence of preclinical cerebellar amyloid plaque deposition in autosomal dominant Alzheimer's disease-causing Presenilin-1 E280A mutation carriers. Neuroimage Clin 2021;31:102749 PMID: 34252876. doi:10.1016/j.nicl.2021.102749.
[56] Shimada H, Minatani S, Takeuchi J, et al. Heavy Tau burden with subtle amyloid β accumulation in the cerebral cortex and cerebellum in a case of familial Alzheimer's disease with APP Osaka Mutation. Int J Mol Sci 2020;21(12) PMID: 32580499. doi:10.3390/ijms21124443.
[57] Salloway S, Honigberg LA, Cho W, et al. Amyloid positron emission tomography and cerebrospinal fluid results from a crenezumab anti-amyloid-beta antibody double-blind, placebo-controlled, randomized phase II study in mild-to-moderate Alzheimer's disease (BLAZE). Alzheimers Res Ther 2018;10(1):96 PMID: 30231896. doi:10.1186/s13195-018-0424-5.
[58] Salloway S, Farlow M, McDade E, et al. A trial of gantenerumab or solanezumab in dominantly inherited Alzheimer's disease. Nat Med 2021;27(7):1187–96 PMID: 34155411. doi:10.1038/s41591-021-01369-8.